Atmospheric Research 277 (2022) 106317

Contents lists available at ScienceDirect

Atmospheric Research

journal homepage: www.elsevier.com/locate/atmosres

Spatio-temporal variability of cloud top and tropopause heights over the Arctic from 10-year CALIPSO, GPSRO and MERRA-2 datasets

Huidong Yeo [a], Hataek Kwon [a,*], Joowan Kim [b], Ho-Young Ku [c], Man-Hae Kim [a], Sang-Woo Kim [a,*]

[a] School of Earth and Environmental Sciences, Seoul National University, Seoul 08826, Republic of Korea
[b] Department of Atmospheric Science, Kongju National University, Kongju 32588, Republic of Korea
[c] Division of Earth Environmental System Sciences Major of Environmental Atmospheric Science, Pukyong National University, Pusan 32588, Republic of Korea

ARTICLE INFO

Keywords:
Cloud top height
Tropopause height
CALIPSO
GPSRO
Arctic cloud

ABSTRACT

The characteristics of cloud top heights (CTHs) and tropopause heights (TPHs) over the Arctic and their relationship were investigated using Cloud-Aerosol Lidar Infrared Pathfinder Satellite (CALIPSO) observations and Modern-Era Retrospective Analysis for Research and Applications, Version 2 (MERRA-2) data for approximately 10 years from June 2006 to March 2016. Global positioning system radio occultation (GPSRO) measurements were also used to validate the TPHs derived from the MERRA-2 reanalysis data. Results of the composite analysis indicate that CTHs over the Arctic generally constitute the low-top (lower than ~3 km) and high-top (higher than ~7 km) categories in all seasons. The high CTHs above approximately 8 km show a close relationship with TPHs in all seasons, with an especially strong positive correlation in winter. In general, both CTH and TPH for each season revealed by composite analysis exhibited a zonally symmetric pattern with greater heights at lower latitudes, except for the winter when significantly high CTHs and TPHs were observed in the Greenland Sea, Atlantic, and Scandinavian regions. The proportion of high CTHs in these regions was higher than that in other regions. Notably, CTH values in the range of approximately 9.7–10.5 km over these regions are slightly higher than the climatological TPHs in winter. From a detailed analysis of Atlantic storm tracks, we conclude that the Atlantic windstorms make a significant contribution to the higher CTHs and TPHs over the Norwegian, Greenland, Kara-Barents Seas, and Northwest Russian regions of the Arctic.

1. Introduction

The Arctic is a cloudy region with an annual average cloud cover of approximately 70% (Eastman and Warren, 2010; Yeo et al., 2022). Arctic clouds significantly influence the Arctic and global climates through radiation feedback between the sea ice and clouds (Pavolonis and Key, 2003) and the subsequent large-scale changes in atmospheric circulation (Kay et al., 2016). Previous studies have investigated the geometric and microphysical properties of clouds and cloud-radiation feedback from ground-based (Dong et al., 2010; Shupe et al., 2011; Cho et al., 2021), ship-based (Intrieri et al., 2002; Achtert et al., 2020), and satellite measurements (Chan and Comiso, 2013); however, the study of cloud parameters remains challenging because of the complexity of cloud microphysical processes (Morrison et al., 2012; Sotriopoulou et al., 2020; Yeo et al., 2022) and lack of reliable observations particularly over the Arctic (Kay et al., 2016).

To comprehensively understand Arctic cloud-radiation feedback mechanisms, in-situ and remotely sensed datasets such as cloud fraction, height, thickness, phase, and droplet size are crucial (Curry and Ebert, 1992; Francis, 1999). The vertical resolution of the information is also important in estimating how clouds and surface temperature (i.e., sea ice melting) are correlated, because the vertical distributions of the cloud amount and its associated properties determine the strength of downward longwave radiation (Intrieri et al., 2002; Schweiger et al., 2008; Yeo et al., 2018; Morrison et al., 2019; Achtert et al., 2020). For example, Ohring and Adler (1978) showed that a 1 km increase in cloud top height (CTH) would cause an approximate increase of 1.2 K in surface temperature, based on a modeling study. Most studies examining the CTH over the Arctic have focused on the retrieval and validation of CTHs from various satellite measurements over a short period (Weisz et al., 2007; Cheng et al., 2021) rather than physically investigating the spatial and temporal structure of CTHs over the Arctic.

* Correspondence author.
E-mail addresses: dixon409@snu.ac.kr (H. Kwon), sangwookim@snu.ac.kr (S.-W. Kim).

https://doi.org/10.1016/j.atmosres.2022.106317
Received 26 March 2022; Received in revised form 18 June 2022; Accepted 21 June 2022
Available online 26 June 2022

Meanwhile, the radiative effect of clouds is known to play a significant role in the thermal and dynamical structures of the upper troposphere and lower stratosphere (Fueglistaler and Fu, 2006; Yang et al., 2010; Pan and Munchak, 2011). Yang et al. (2010) investigated the radiative impact of clouds in the tropopause, while Pan and Munchak (2011) examined the influence of the tropopause on CTH and showed that the thermal tropopause appears to be a significant constraint on the maximum cloud height. However, these analyses were focused on the tropics and mid-latitudes, and the relationship between CTH and tropopause is still unknown over the Arctic.

In this study, we investigated the characteristics of the spatial and temporal structures of both CTHs and tropopause heights (TPHs) over the Arctic using the Cloud-Aerosol Lidar and Infrared Pathfinder Satellite Observations (CALIPSO) and Global Positioning System Radio Occultation (GPSRO) measurements, together with the Modern-Era Retrospective Analysis for Research and Applications, Version 2 (MERRA2) reanalysis, for approximately 10 years from June 2006 to March 2016. We also analyzed Atlantic storm track data to investigate the possible cause of the exceptionally high cloud distribution over the Atlantic sector of the Arctic during winter. The following sections of this study are organized as follows. Section 2 describes the data and methods used in this study, while the results of the climatology of TPHs and the composite of CTHs over the Arctic are presented in Sections 3 and 4. The contribution of Atlantic storms to the elevated CTH over the Arctic is discussed in Section 5, followed by a discussion of results and summary in the last section.

2. Data and methods

2.1. CALIPSO observation

The CTH was examined based on the Cloud-Aerosol Lidar with Orthogonal Polarization (CALIOP) onboard the CALIPSO. CALIOP provides cloud observations equatorward of 82° N owing to its orbit inclination and narrow field-of-view (Winker et al., 2017). Therefore, the CTHs over the region between 60° N and 82° N were investigated in this study. Because CALIOP observations at 532 and 1064 nm channels can identify optically thin clouds at high altitudes (e.g., cirrus), they can be used to investigate clouds near the tropopause over the Arctic, where deep convection rarely occurs compared to the tropics or mid-latitudes.

In this study, CTH is defined as the top height of the highest layer identified as clouds in the version 4 (V4) CALIOP level 2, 5 km cloud layer (L2_05kmCLay) product. However, clouds with a top height exceeding 15 km are excluded from this study since the generic "stratospheric layer" in CALIOP retrievals has been eliminated in V4 (Liu et al., 2019). We used the CTH from every single profile of observations for comparison with TPH, and the area mean value of CTH over a 2° × 2° longitude-latitude grid is also computed for the analysis of the temporal and spatial variability of CTH.

TPH information included in the CALIPSO product as part of ancillary data was used in this study. The TPH given in the CALIPSO cloud layer data product is based on the Modern-Era Retrospective Analysis for Research and Applications, Version 2 (MERRA-2) reanalysis data (Young et al., 2018) and interpolated along the CALIPSO orbit track. The MERRA2 reanalysis is generated a 0.625° × 0.5° longitude-latitude resolution at 72 layers between the surface and 0.01 hPa. In MERRA2 reanalysis, approximately 3 million observations per 6-h cycle were assimilated, including temperature profiles from radiosondes, aircraft measurements, and GPSRO observations (bending angle) for the tropopause region (Wargan and Coy, 2016). The global TPHs in MERRA2 are well reproduced with little bias, compared to radiosonde observations (Xian and Homeyer, 2019).

2.2. GPSRO observation

The TPH and thermal structure near the tropopause were examined using global positioning system (GPS) radio occultation (RO) measurements. GPSRO measurements provide temperature profiles with a high vertical resolution (0.1 km near the surface to 1 km near the tropopause) in the upper troposphere and stratosphere with unprecedented accuracy and sampling frequency, particularly over the Arctic. The GPSRO measurements are known to have high accuracy (equivalent to <1 K; average accuracy <0.1 K) and precision (0.02–0.05 K) (Anthes, 2011) for a temperature in the vertical range of 10–40 km, and equal accuracy over the land and the ocean (Cucurull et al., 2013). The most powerful benefits of GPSRO measurements are no satellite bias and minimal effect of clouds or precipitation on the data, compared to other satellite observations (Kwon et al., 2015).

Approximately 10 years of temperature data from June 2006 to March 2016 were obtained from the Constellation Observing System for Meteorology, Ionosphere, and Climate (COSMIC) GPSRO mission (Anthes et al., 2008). The TPH was computed using the GPSRO temperature profiles using the algorithm proposed by Reichler et al. (2003), based on the definition of the World Meteorological Organization (WMO, 1957); it is generally called lapse-rate tropopause (LRT) and is defined as "the lowest level at which the lapse-rate decreases to 2 °C/km or less, and average lapse-rate between this level and all higher levels within 2 km does not exceed 2 °C/km.". The algorithm of Reichler et al. (2003) is applicable to both low- and high-resolution temperature profiles. In general, TPH estimation from GPSRO measurements is not sensitive to algorithms owing to its high-resolution features.

2.3. Detection of Atlantic storm track

To investigate the impact of Atlantic storms on the CTHs over the Arctic, we detected Atlantic storms using the Japanese 55-year Reanalysis (JRA-55; Kobayashi et al., 2015) for June 2006–March 2016. The relative vorticity at 850-hPa and mean-sea level pressure with a spatial resolution of 1.25° latitude and 1.25° longitude were used to detect Atlantic storms in this study. The Atlantic storm detection and tracking method used in this study is based on Hong et al. (2020), and optimized for Northern Hemisphere extratropical storm detection. This method is a modified version of the method described by Vitart et al. (1997). The procedure for the detection of Atlantic storms is as follows:

(1) 6-hourly storm center candidates are detected using the local maximum of the 850-hPa relative vorticity ($< 2.0 \times 10^{-5}$ s^{-1}) and the closest local minimum of the mean sea level pressure within a 400 km radius of the local vorticity maximum.
(2) The storm center candidates track the next storm center within a circular tracking boundary with a radius of 750 km, and the location of the storm at each time step is set as the center of the tracking boundary.
(3) Finally, connecting the storm center candidates in sequence generates the entire life cycle of each storm.

In this study, the cyclogenesis region was set to 25–65° N and 30° W–30° E, and storms were filtered based on minimum lifetime (threshold <48 h) and minimum distance traveled (threshold <1000 km).

3. 10-year climatology of TPH over the Arctic

Fig. 1 shows the horizontal distributions of seasonal TPH from CALIPSO-MERRA2 and GPSRO observations for 10 years, from June 2006 to March 2016. TPHs from CALIPSO-MERRA2 show a zonally symmetric horizontal distribution with values of approximately 8–11 km in all seasons except winter. The zonally symmetric feature of TPH was the most pronounced in summer, with the largest values ranging from approximately 9 km at high latitudes to 11 km at lower latitudes, among the four seasons. The minimum value (~7.9 km) of the TPH appears mainly over the Baffin Bay and the Ellesmere Islands (~75° N,

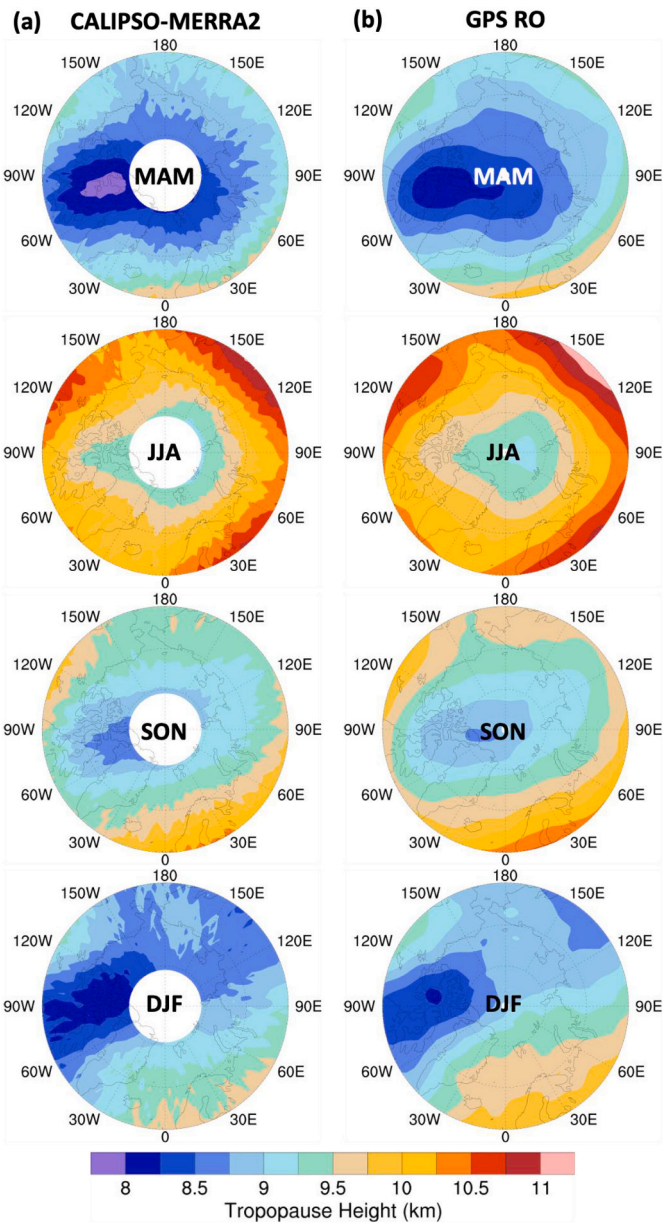

Fig. 1. Seasonal climatology of tropopause height derived from (a) CALIPSO-MERRA2 (left column) and (b) GPSRO (right column) for June 2006–March 2016.

~90° W) in spring, with approximate values ranging from 7.9 to 9.7 km. The TPH appears lower in the western hemisphere than in the eastern hemisphere. The spatial distribution was zonally more asymmetric during fall than in summer, similar to the springtime distribution but with higher values. The spatial patterns of the TPH in winter differed the most from those in other seasons. There is a strong asymmetry of the TPH in the zonal direction over the Greenland, Atlantic, and Scandinavian regions (30° W–90° E). The TPH over this region is approximately 9–9.5 km, which is higher than that in other regions. The overall pattern of seasonal TPH climatology is qualitatively consistent with the climatology of tropopause pressure derived from ERA reanalysis and radiosonde data from previous studies (e.g., Highwood et al., 2000).

To validate the TPH derived from CALIPSO-MERRA2, it was compared with the TPHs derived from GPSRO observations. It is known that the temperature profiles in the upper troposphere and lower stratosphere provided by the GPSRO observation system are highly accurate (Kursinski et al., 1997; Anthes et al., 2008; He et al., 2009) and has been widely used in research on the global tropopause (Grise et al., 2010; Son et al., 2011; Rieckh et al., 2014). The TPHs derived from CALIPSO-MERRA2 observations generally showed good agreement with the TPHs derived from GPSRO observations in terms of seasonal spatial patterns as well as TPH values for all seasons (Fig. 1). Compared to other seasons, the spatial distribution of TPH in winter presents a larger difference. The TPHs from the GPSRO measurements is higher than those from CALOPSO-MERRA2 over the Kara-Barents Sea, Europe, and western Siberia. A small systematic offset was observed between the two datasets; the TPH derived from GPSRO showed a slightly higher value than that from the CALIPSO-MERRA2 dataset. This can be clearly seen in the scatter plots of TPHs derived from CALIPSO-MERRA2 and GPSRO observations, depending on the distance between the observation points of the two datasets (Fig. 2). Since the observation points of the two datasets are not identical, the GPSRO observations nearest to the CALIPSO-MERRA2 observation were used to compare the TPHs. The difference between two TPH observations is quantitatively examined depending on the distance of 50, 100, and 200 km between GPSRO and CALIPSO-MERRA2 observation points. The TPHs from CALIPSO-MERRA2 and GPSRO show good agreement, with a correlation coefficient >0.85 for all three cases. The comparison for distances <100 km showed better agreement between the two datasets, with a correlation coefficient of 0.88. TPHs derived from CALIPSO-MERRA2 showed a negative, but the small statistical bias of approximately 0.11 km (mean value of a, b, and c) and a root mean square deviation of approximately 0.7 km (mean value of a, b, and c) relative to TPHs from GPSRO. This result supports our choice of CALIPSO tropopause products for the following CTH analysis.

4. CTH and its relationship to TPH over the Arctic

We compared the CTH and TPH to examine their relationship over the Arctic. Fig. 3 shows scatter plots for TPHs derived from CALIPSO-MERRA2 and CTH derived from CALIPSO observations, for each season from June 2006 to March 2016. It may be noted that only TPH and CTH observations corresponding to the same time and location were compared. The samples are well grouped by low and high CTH values, generally for all seasons. The low CTHs appear at a vertical level of approximately <3 km, and the high CTHs appear at the vertical level of approximately 7–10 km. It is known that the Arctic is mainly covered with low-lying clouds (Curry et al., 1996), but Fig. 3 reveals that a considerable amount of high clouds exist above 7 km in the Arctic region. It has been reported that Arctic clouds induce surface warming except for summer (Ebell et al., 2020). Low-level clouds are an important factor for surface radiation budget by increasing downward longwave radiation up to 83 W m^{-2} when low-level clouds occur (Yeo et al., 2018). In addition to their radiative effects, high-level clouds (i.e., cirrus) can affect trace gas concentration (e.g., reactive nitrogen) near the tropopause and, consequently local ozone concentration (Voigt et al., 2006).

In the scatter plots shown in Fig. 3, high CTHs (> 8 km) are well constrained by TPHs. Especially in winter, a strong positive correlation between high CTHs and TPHs compared to other seasons is observed, and the proportion of high clouds is much higher than that of low-level clouds. This result is consistent with the observations of a previous study— based on CloudSat-CALIPSO merged data—where the frequency distribution of CTH over the Arctic exhibited bimodal distribution in all seasons and suggested a possible relationship between higher CTH and TPH (Liu et al., 2012).

Based on the robust relationship between CTH and TPH over an altitude of approximately 8 km, we analyzed the spatial structure of CTH of high clouds with CTH larger than 8 km. Fig. 4 shows the seasonal composite CTHs from CALIPSO observations within the vertical altitude range of 8–15 km. It may be noted that only data corresponding to the actual detection of clouds by CALIPSO have been included in Fig. 4. In general, the overall spatial distribution of CTH is similar to that of TPH

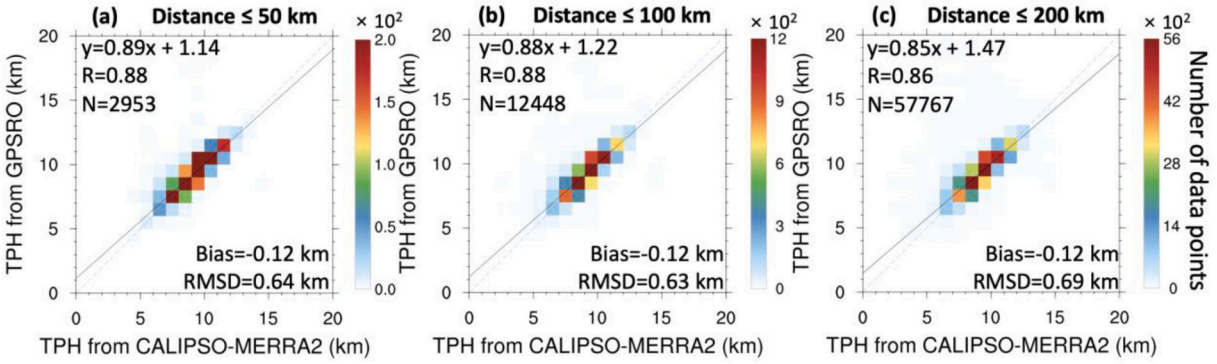

Fig. 2. Comparison of tropopause heights derived from CALIPSO-MERRA2 and GPSRO observations for June 2006–March 2016. Each figure shows comparison of tropopause heights for different distances of GPSRO observation point from CALIPSO-MERRA2 observation point.

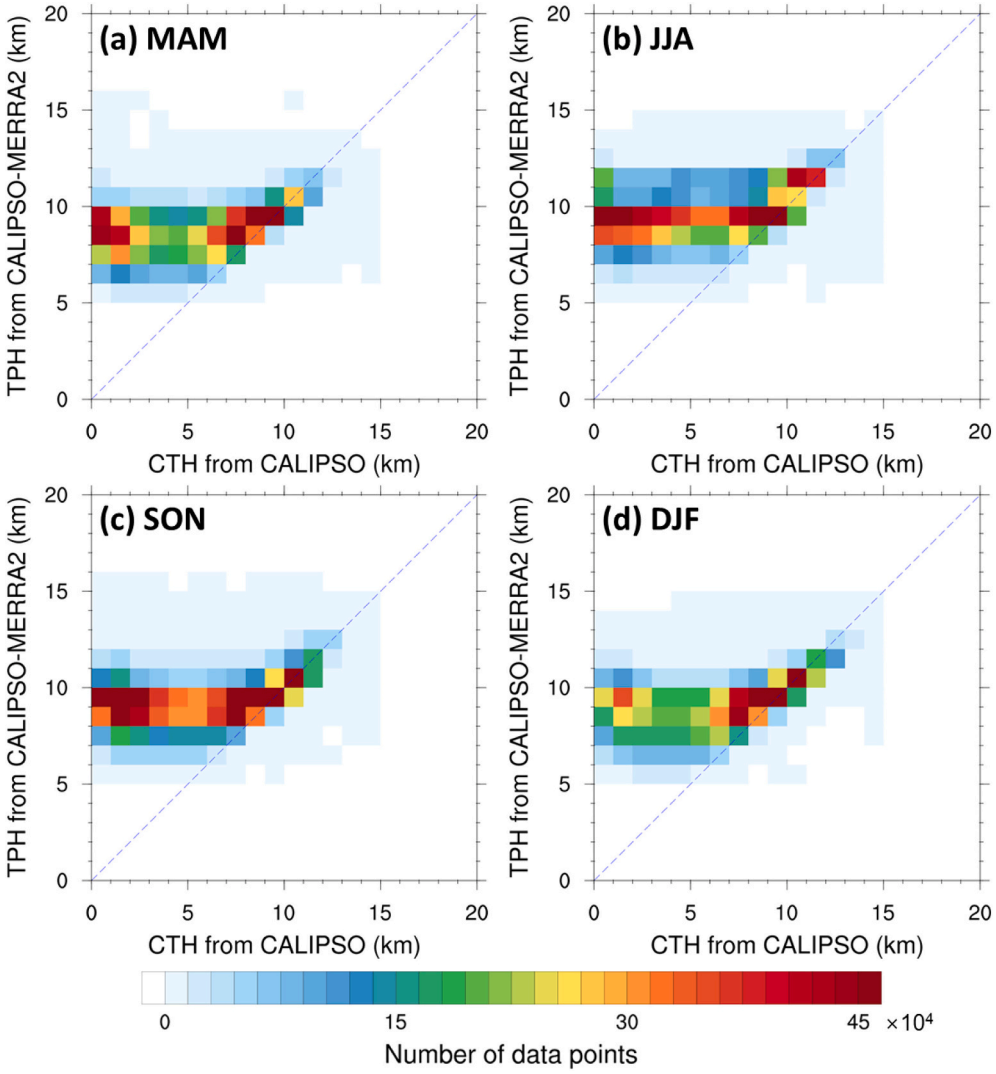

Fig. 3. Scatter plot of tropopause height derived from CALIPSO-MERRA2 and cloud top height derived from CALIPSO observation for four seasons from June 2006 to March 2016.

in all seasons, with values in the range of approximately 8.5–11 km, as seen in Fig. 1. The CTH in spring and summer exhibits zonally symmetric patterns, with higher values at lower latitudes. The CTH in summer shows a larger value than in other seasons with values in the range of approximately 9.3–11 km, while the lowest CTHs are seen during spring. The zonally symmetric feature of the CTH patterns becomes weaker in the fall and disappears in winter. An interesting feature of the wintertime CTH is notably high CTH values over the Greenland Sea, Atlantic, and Scandinavian regions (30° W–90° E) where the CTH (~ 9.7–10.5 km) is higher than that indicated in the TPH climatology. In addition, the CTHs are higher in winter than in summer only in these regions. This implies that high clouds could exist above the tropopause during the

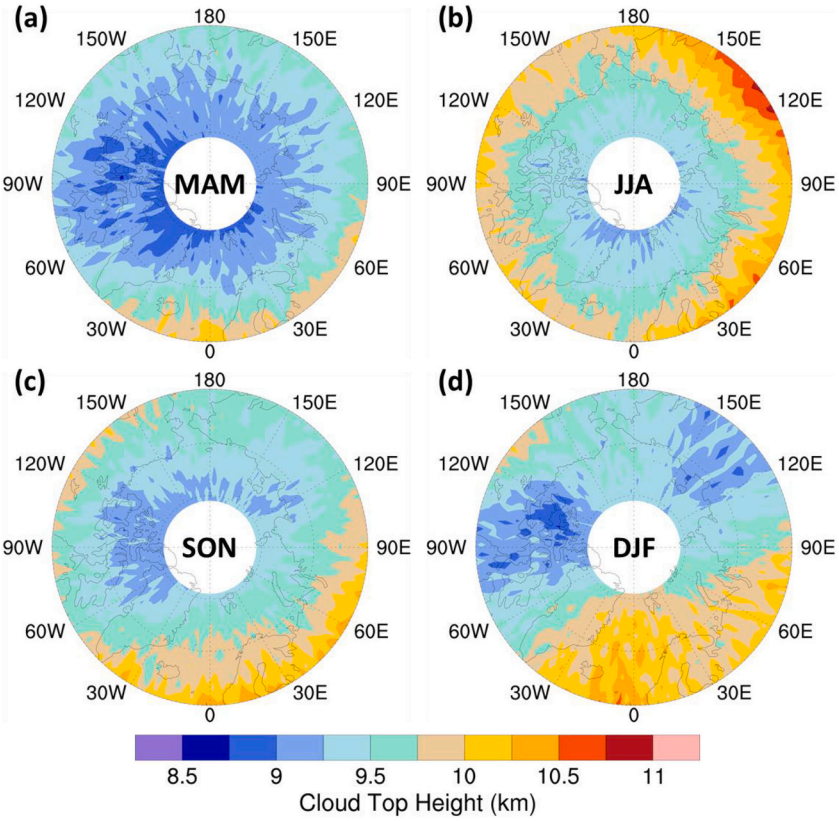

Fig. 4. Seasonal composite cloud top height derived from CALIPSO observations within vertical range of 8–15 km for June 2006–March 2016. (a), (b), (c) and (d) each shows composite map for one season.

Arctic winter, particularly over the regions. These high clouds are known to be related to active deep convection, based on previous analyses and observations (Liu et al., 2007; Yang et al., 2010), and are accompanied by Atlantic storms passing through these regions. Atlantic storms usually are generated over the western Atlantic and travel northeast over time, with intense storms moving as far as the North Pole. We examined Atlantic storm track activity, which we considered as one of the possible causes for the high cloud top observed over the Atlantic side of the Arctic in winter.

5. Contribution of Atlantic storms to the elevated CTH over the Arctic

In order to demonstrate the typical changes in the CTH and TPH associated with the Atlantic storm intruding into the Arctic, the time-height cross-section of the backscattering, TPHs, and temperature from CALIPSO dataset are examined for two strong and typical Atlantic storms entrancing into the Arctic (Fig. 5); the events occurred in January 2010 and 2016, respectively. The storm event in January 2016 (Fig. 5b), named 'Frank' by the U.K. Met office, recorded a minimum central pressure of 928 hPa on December 30, 2015, and is known to have triggered the unprecedented abrupt warming in January 2016 by bringing enormous masses of moist warm air to the Arctic (Kim et al., 2017). In both storm cases, the high CTH values ranging from approximately 8–13 km matched well with the TPHs. Fig. 6 shows the Atlantic storm tracks for four seasons from June 2006 to March 2016, indicating storm tracks within the top 10% of storm intensity. It can be seen that most of the intense storms within the top 10% category—considering storms in all seasons—are observed in winter; 49 of the 192 storms detected in winter belonged to this category. In contrast, strong Atlantic storms were rarely observed during the other seasons. No Atlantic storms within the top 10% in intensity were detected in summer, and only six strong windstorms were detected in spring. The strong storms (blue solid lines) detected in winter, shown in Fig. 6d, traveled over the Arctic region above 60° N. Previous studies have shown that stronger Atlantic storms tend to deflect poleward while weaker storms tend to move northeastward to the Atlantic sector of the Arctic Ocean; these strong storms are known to bring enormous amounts of warm and moist air into the Arctic during storm events (Hong et al., 2020). Most storms move to the Arctic region through the Norwegian Sea (30° W–0° longitude, ~60° N latitude), remain in the Arctic region (30° W–60° E longitude and 60° N–75° N latitude), and then disappear. The fact that the Arctic region is affected by Atlantic storms is consistent with the region exhibiting high CTHs and TPHs in winter, as shown in Figs. 1(DJF) and Fig. 4d.

Fig. 7 shows the composite of CTH and TPH derived from CALIPSO observations for the days from when the Atlantic storms enter the Arctic circle (60° N) to when they disappear inside the Arctic. A noticeable feature in Fig. 7a is the high CTH values of approximately 10–11 km in the Atlantic sector of the Arctic Ocean including the Norwegian, Greenland, Kara-Barents Seas, and Northwest Russian regions. This suggests a correspondence between the CTH in the Atlantic sector of the Arctic Ocean and the Atlantic windstorms prevailing in the region. Atlantic windstorms that cross the Arctic circle tend to disappear over the Greenland Sea, but the highest values of CTH are observed over the Kara Sea and Northwest Russia. Also, in the CTH composite map for the storms within the top 10% of intensity, the peak value of high CTH appears mostly in the Kara-Barents Sea area (not shown). Considering that warm and humid air is brought northward by a warm front accompanied by a cyclone system, the observation of the highest value of CTH over the Kara-Barents Sea suggests that a sudden inflow of warm and humid air along with a warm front located east of the center of the storm contributes to the high CTH over the region. The TPH in the composite map depicted in Fig. 7b shows a spatial distribution very similar to that of the CTH, as shown in Fig. 7a, with the regions showing

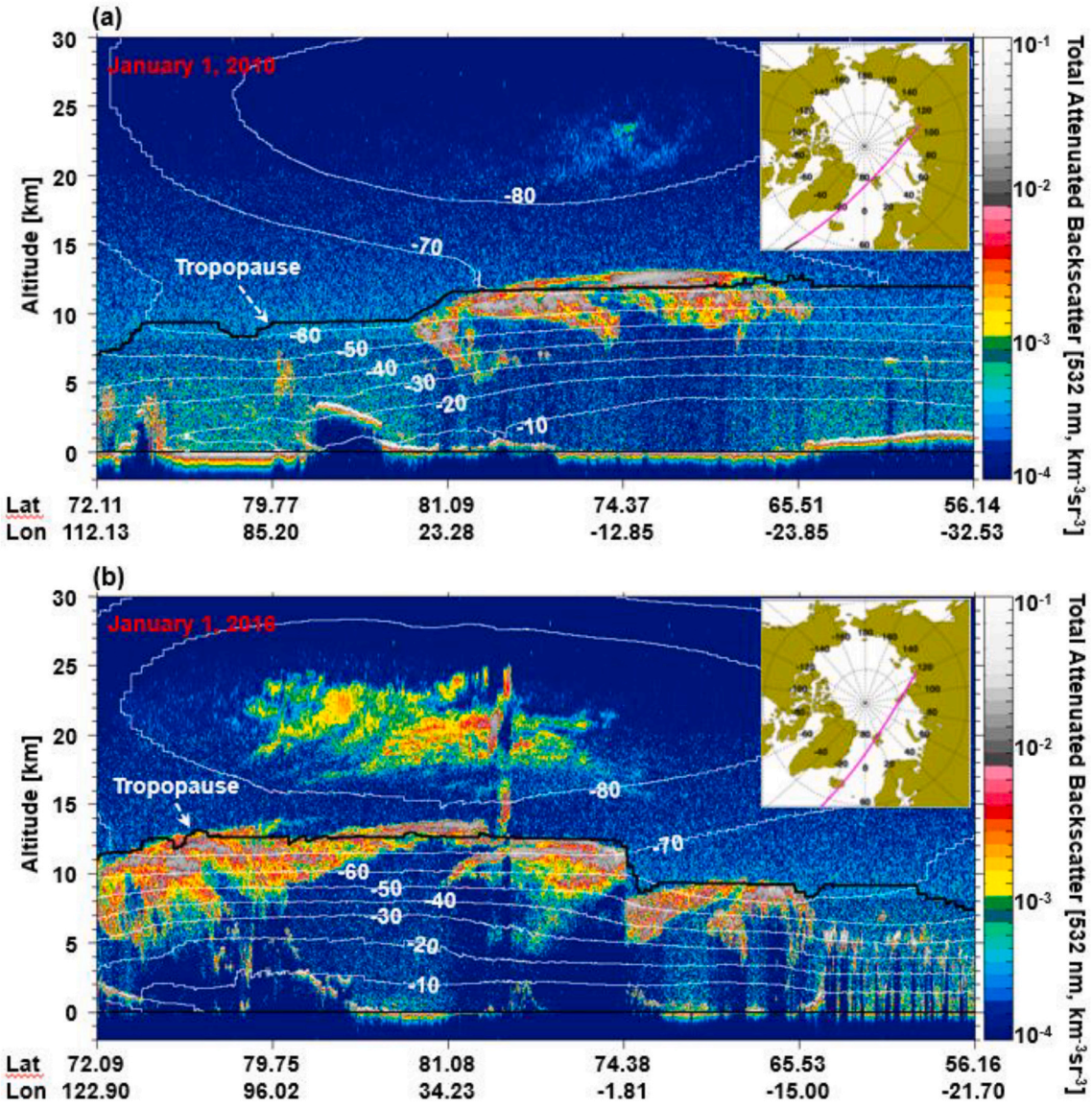

Fig. 5. Time-height image of total attenuated backscatter (shading), tropopause (bold black line), and temperature (white lines) from CALIPSO dataset for two cases of Atlantic storm on January 1 of (a) 2010 and (b) 2016.

high TPH values well matched with the high CTH region. These results suggest that, like the CTH, the high values of TPH over the Norwegian, Greenland, Kara-Barents Seas, and Northwest Russian regions are also associated with the Atlantic storms entering the Arctic regions.

6. Discussion and summary

In this study, we investigated the characteristics of CTHs and TPHs over the Arctic using CALIPSO and GPSRO observations for the period of June 2006–March 2016. Clouds over the Arctic are characterized by clear distinctions between the lower cloud with a CTH lower than 3 km and the upper cloud with a CTH higher than approximately 7 km in all seasons except winter. In winter, the CTH was mostly distributed in the vertical range of approximately 7–10 km.

Typically, the seasonal mean distribution of the CTH exhibits a largely symmetric pattern in the zonal direction, with a higher height in the lower latitudes. The CTH in summer shows a larger value than in other seasons with values in the approximate range of 9.3–11 km. In contrast, a considerable asymmetric pattern of CTH is found over the Greenland Sea, Atlantic, and Scandinavian regions (30° W–90° E longitude, 60° N–80° N latitude), especially in the Arctic winter. The CTHs over this area show a slightly higher value than the TPH climatological values of approximately 9.5–10.2 km. The structure of the seasonal TPH climatology derived from CALIPSO-MERRA2 is generally similar to that of the CTH in all seasons, with values of approximately 8–11 km.

We also examined the relationship between high CTH and TPH values derived from CALIPSO-MERRA2 and GPSRO observations over the Arctic region. We found that high CTHs above approximately 8 km were closely related to the TPH in all seasons. Especially, a more robust relationship between high CTHs and TPHs was found in winter compared to other seasons. High CTHs above approximately 10 km in the Arctic winter are concentrated over the Greenland Sea, Atlantic, and Scandinavian regions (30° W–90° E longitude, 60° N–80° N latitude).

The contribution of Atlantic storms to the elevated CTH and TPH values over the Arctic in winter was investigated by detecting Atlantic storm tracks passing through high CTH and TPH regions. We found that approximately 66% (49) of strong storms within the top 10% of intensity were detected in winter, and that these intense storms entered the Arctic through the Norwegian and Greenland Seas, dissipating within the

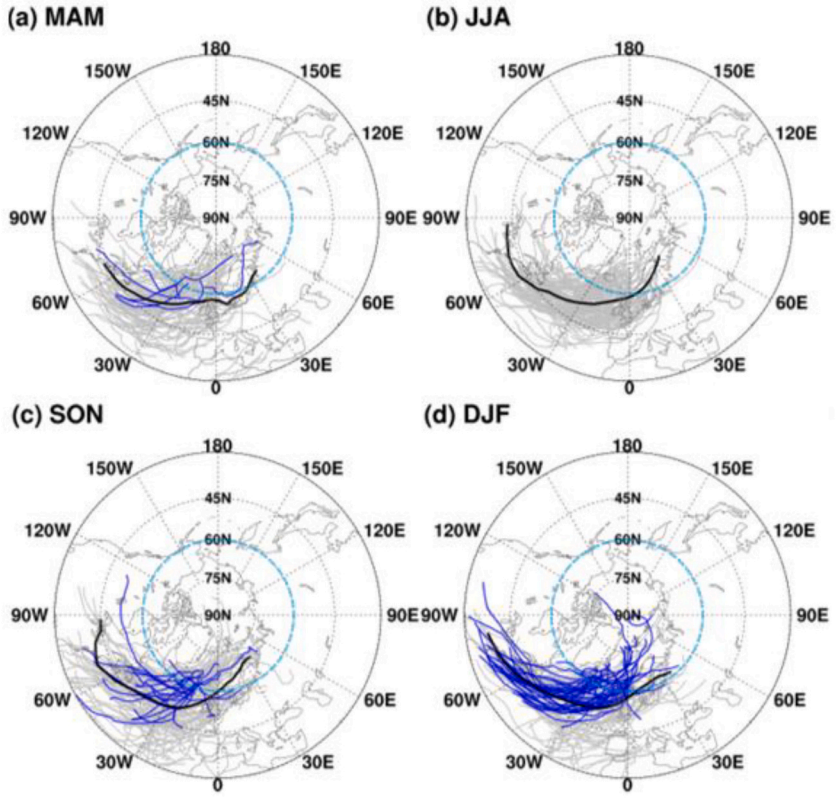

Fig. 6. Atlantic windstorm tracks for four seasons during June 2006–March 2016. Grey and blue lines indicate all detected storm tracks in each season and storm tracks of Atlantic windstorms within top 10% strength in all seasons, respectively. Bold black line indicates mean track of Atlantic windstorms for each season. (For interpretation of the references to colour in this figure legend, the reader is referred to the web version of this article.)

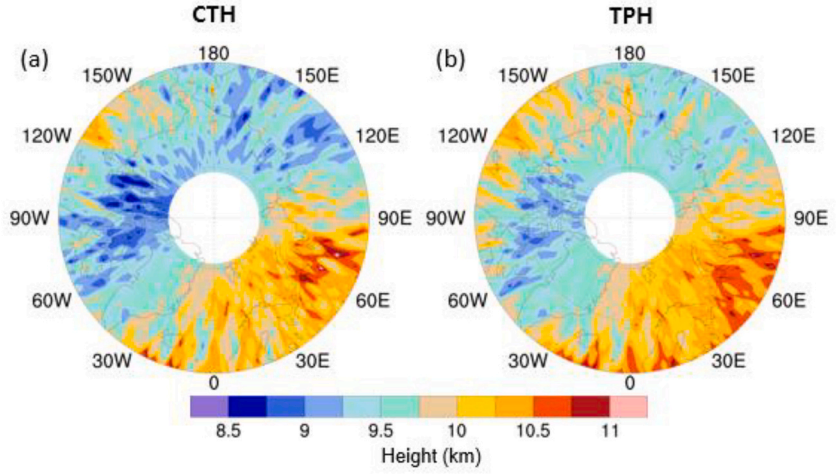

Fig. 7. Composite map of (a) cloud top height and (b) tropopause height derived from CALIPSO observations for days from when Atlantic storms entered the Arctic circle (60° N) to when they disappeared inside the Arctic in winter from June 2010–to March 2016.

Arctic region. In addition, the Arctic region showing high CTHs and TPHs in winter is also indicative of the region being affected by Atlantic storm tracks. The composite analysis of the CTH for the days from when the Atlantic storms enter the Arctic circle (60° N) and to when they disappear inside the Arctic indicates high CTH values of approximately 10–11 km in the Atlantic sector of the Arctic Ocean, including over the Norwegian, Greenland, Kara-Barents Seas, and Northwest Russian regions. Regions showing a high TPH value in the composite map of TPHs matched well with the high CTH region. This suggests a correspondence between the CTH and TPH in the Atlantic sector of the Arctic Ocean, and the influence of prevailing Atlantic storms. Although this study mainly focuses on the role of Atlantic storms in lifting the CTH and TPH in the Atlantic sector of the Arctic (Fig. 3), it also observes that the CTH and TPH in the Arctic region exhibit the highest values over the Norwegian Sea. This is thought to be related to the cyclone activity occurring in the Icelandic low system, which is known as a major area of cyclogenesis. Therefore, a complete understanding of the elevated CTH and TPH requires the simultaneous consideration of contributions from lee cyclogenesis leading to the Greenland and Atlantic storms. Further investigation is needed on the effect of cyclone activity in the Icelandic

low on high CTHs in the Norwegian Sea region.

Data availability

CALIPSO datasets related to this article can be obtained from the NASA Langley Research Center and Atmospheric Science Data Center (https://asdc.larc.nasa.gov/). The COSMIC GPSRO data is available at University Corporation for Atmospheric Research (UCAR) COSMIC data archive (doi:https://doi.org/10.5065/ZD80-KD74). The Japanese 55-year Reanalysis (JRA-55) data is openly available from NCAR data server (doi:https://doi.org/10.5065/D6HH6H41).

CRediT authorship contribution statement

Huidong Yeo: Visualization, Formal analysis, Writing – review & editing. **Hataek Kwon:** Conceptualization, Writing – original draft. **Joowan Kim:** Formal analysis, Writing – review & editing. **Ho-Young Ku:** Visualization, Formal analysis, Writing – review & editing. **Man-Hae Kim:** Visualization, Writing – review & editing. **Sang-Woo Kim:** Conceptualization, Writing – review & editing.

Declaration of Competing Interest

The authors declare no conflict of interest.

Acknowledgments

This work was supported by the R&D Program for Oceans and Polar Regions of the National Research Foundation (NRF) funded by the Ministry of Science and ICT (2020M1A5A1110579), and the National Research Foundation of Korea (NRF) grant funded by the Korea government (NRF-2020R1A2C1014679). Joowan Kim was supported by the National Research Foundation of Korea (NRF-2020R1F1A1075859).

References

Achtert, P., O'Connor, E.J., Brooks, I.M., Sotiropoulou, G., Shupe, M.D., Pospichal, B., Brooks, B.J., Tjernström, M., 2020. Properties of Arctic liquid and mixed-phase clouds from shipborne Cloudnet observations during ACSE 2014. Atmos. Chem. Phys. 20, 14983–15002. https://doi.org/10.5194/acp-20-14983-2020.

Anthes, R.A., 2011. Exploring Earth's atmosphere with radio occultation: contributions to weather, climate and space weather. Atmos. Meas. Tech. 4 (6), 1077–1103. https://doi.org/10.5194/amt-4-1077-2011.

Anthes, R.A., Bernhardt, P.A., Chen, Y., Cucurull, L., Dymond, K.F., Ector, D., Healy, S.B., Ho, S.-P., Hunt, D.C., Kuo, Y.-H., Liu, H., Manning, K., McCormick, C., Meehan, T.K., Randel, W.J., Rocken, C., Schreiner, W.S., Sokolovskiy, S.V., Syndergaard, S., Thompson, D.C., Trenberth, K.E., Wee, T.-K., Yen, N.L., Zeng, Z., 2008. The COSMIC/FORMOSAT-3 Mission: early results. Bull. Amer. Meteor. Soc. 89, 313–333. https://doi.org/10.1175/BAMS-89-3-313.

Chan, M.A., Comiso, J.C., 2013. Arctic cloud characteristics as derived from MODIS, CALIPSO, and CloudSat. J. Clim. 26 (10), 3285–3306. https://doi.org/10.1175/JCLI-D-12-00204.1.

Cheng, X., Yi, L., Bendix, J., 2021. Cloud top height retrieval over the Arctic Ocean using a cloud-shadow method based on MODIS. Atmos. Res. 253, 105468 https://doi.org/10.1016/j.atmosres.2021.105468.

Cho, Y., Park, S.-J., Kim, J.-H., Yeo, H., Nam, J., Jun, S.-Y., Kim, B.-M., Kim, S.-W., 2021. Investigating wintertime cloud microphysical properties and their relationship to air mass advection at Ny-Ålesund, Svalbard using the synergy of a cloud radar–Ceilometer–Microwave Radiometer. Remote Sens. 13 (13), 2529. https://doi.org/10.3390/rs13132529.

Cucurull, L., Derber, J.C., Purser, R.J., 2013. A bending angle forward operator for global positioning system radio occultation measurements. J. Geophys. Res. Atmos. 118 (1), 14–28. https://doi.org/10.1029/2012JD017782.

Curry, J.A., Ebert, E.E., 1992. Annual cycle of radiation fluxes over the Arctic Ocean: sensitivity to cloud optical properties. J. Clim. 5 (11), 1267–1280. https://doi.org/10.1175/1520-0442(1992)005%3C1267:ACORFO%3E2.0.CO;2.

Curry, J.A., Schramm, J.L., Rossow, W.B., Randall, D., 1996. Overview of Arctic cloud and radiation characteristics. J. Clim. 9 (8), 1731–1764. https://doi.org/10.1175/1520-0442(1996)009%3C1731:OOACAR%3E2.0.CO;2.

Dong, X., Xi, B., Crosby, K., Long, C.N., Stone, R.S., Shupe, M.D., 2010. A 10 year climatology of Arctic cloud fraction and radiative forcing at Barrow, Alaska. J. Geophys. Res. Atmos. 115, D17. https://doi.org/10.1029/2009JD013489.

Eastman, R., Warren, S.G., 2010. Interannual variations of Arctic cloud types in relation to sea ice. J. Clim. 23, 4216–4232. https://doi.org/10.1175/2010JCLI3492.1.

Ebell, K., Nomokonova, T., Maturilli, M., Ritter, C., 2020. Radiative effect of clouds at Ny-Ålesund, Svalbard, as inferred from ground-based remote sensing observations. J. Appl. Meteorol. Climatol. 59 (1), 3–22. https://doi.org/10.1175/JAMC-D-19-0080.1.

Francis, J., 1999. Cloud radiative forcing over Arctic surfaces. In: Proceedings 5th Conference on Polar Meteorology and Oceanography, pp. 221–226.

Fueglistaler, S., Fu, Q., 2006. Impact of clouds on radiative heating rates in the tropical lower stratosphere. J. Geophys. Res. Atmos. 111 (D23).

Grise, K.M., Thompson, D.W.J., Birner, T., 2010. A global survey of static stability in the stratosphere and upper troposphere. J. Clim. 23, 2275–2292. https://doi.org/10.1175/2009JCLI3369.1.

He, W., Ho, S., Chen, H., Zhou, X., Hunt, D., Kuo, Y.-H., 2009. Assessment of radiosonde temperature measurements in the upper troposphere and lower stratosphere using COSMIC radio occultation data. Geophys. Res. Lett. 36, L17807. https://doi.org/10.1029/2009GL038712.

Highwood, E.J., Hoskins, B.J., Berrisford, P., 2000. Properties of the Arctic tropopause. Q. J. R. Meteorol. Soc. 126, 1515–1532. https://doi.org/10.1002/qj.49712656515.

Hong, J.-Y., Kim, B.-M., Baek, E.-H., Kim, J.-H., Zhang, X., Kim, S.-J., 2020. A critical role of extreme Atlantic windstorms in arctic warming. Asia-Pac. J. Atmospheric Sci. 56, 17–28. https://doi.org/10.1007/s13143-019-00123-y.

Intrieri, J.M., Fairall, C.W., Shupe, M.D., Persson, P.O.G., Andreas, E.L., Guest, P.S., Moritz, R.E., 2002. An annual cycle of Arctic surface cloud forcing at SHEBA. J. Geophys. Res. Oceans 107, C10. https://doi.org/10.1029/2000JC000439.

Kay, J.E., L'Ecuyer, T., Chepfer, H., Loeb, N., Morrison, A., Cesana, G., 2016. Recent advances in Arctic cloud and climate research. Curr. Clim. Change Rep. 2 (4), 159–169. https://doi.org/10.1007/s40641-016-0051-9.

Kim, B.-M., Hong, J.-Y., Jun, S.-Y., Zhang, X., Kwon, H., Kim, S.-J., Kim, J.-H., Kim, S.-W., Kim, H.-K., 2017. Major cause of unprecedented Arctic warming in January 2016: critical role of an Atlantic windstorm. Sci. Rep. 7 (1), 1–9. https://doi.org/10.1038/srep40051.

Kobayashi, Y., Ota, Y., Harada, Y., Ebita, A., Moriya, M., Onoda, H., Onogi, K., Kamahori, H., Kobayashi, C., Endo, H., Miyaoka, K., Takahash, K., 2015. The JRA-55 reanalysis: general specifications and basic characteristics. J. Meteor. Soc. Japan. Ser. II. 93, 5–48. https://doi.org/10.2151/jmsj.2015-001.

Kursinski, E.R., Hajj, G.A., Schofield, J.T., Linfield, R.P., Hardy, K.R., 1997. Observing Earth's atmosphere with radio occultation measurements using the Global Positioning System. J. Geophys. Res.-Atmos. 102 (D19), 23429–23465.

Kwon, H., Kang, J.-S., Jo, Y., Kang, J.H., 2015. Implementation of a GPS-RO data processing system for the KIAPS-LETKF data assimilation system. Atmos. Meas. Tech. 8, 1259–1273. https://doi.org/10.5194/amt-8-1259-2015.

Liu, C., Zipser, E.J., Nesbitt, S.W., 2007. Global distribution of tropical deep convection: different perspectives from TRMM infrared and radar data. J. Clim. 20, 489–503. https://doi.org/10.1175/JCLI4023.1.

Liu, Y., Key, J.R., Ackerman, S.A., Mace, G.G., Zhang, Q., 2012. Arctic cloud macrophysical characteristics from CloudSat and CALIPSO. Remote Sens. Environ. 124, 159–173. https://doi.org/10.1016/j.rse.2012.05.006.

Liu, Z., Kar, J., Zeng, S., Tackett, J., Vaughan, M., Avery, M., Pelon, J., Getzewich, B., Lee, K.-P., Magill, B., Omar, A., Lucker, P., Trepte, C., Winker, D., 2019. Discriminating between clouds and aerosols in the CALIOP version 4.1 data products. Atmos. Meas. Tech. 12, 703–734. https://doi.org/10.5194/amt-12-703-2019.

Morrison, H., de Boer, G., Feingold, G., Harrington, J., Shupe, M.D., Sulia, K., 2012. Resilience of persistent Arctic mixed-phase clouds. Nat. Geosci. 5, 11–17. https://doi.org/10.1038/NGEO1332.

Morrison, H., Kay, J.E., Frey, W.R., Chepfer, H., Guzman, R., 2019. Cloud response to Arctic Sea Ice loss and implications for future feedback in the CESM1 climate model. J. Geophys. Res. Atmos. 124 (2), 1003–1020. https://doi.org/10.1029/2018JD029142.

Ohring, G., Adler, S., 1978. Satellite observations as "Ground Truth" for climate models. In: Advances in Space Exploration. COSPAR Symposium Series (France). Pergamon Press.

Pan, L.L., Munchak, L.A., 2011. Relationship of cloud top to the tropopause and jet structure from CALIPSO data. J. Geophys. Res. Atmos. 116, D12201. https://doi.org/10.1029/2010JD015462.

Pavolonis, M.J., Key, J.R., 2003. Antarctic cloud radiative forcing at the surface estimated from the AVHRR polar pathfinder and ISCCP D1 datasets, 1985–93. J. Appl. Meteorol. Climatol. 42 (6), 827–840. https://doi.org/10.1175/1520-0450(2003)042%3C0827:ACRFAT%3E2.0.CO;2.

Reichler, T., Dameris, M., Sausen, R., 2003. Determining the tropopause height from gridded data. Geophys. Res. Lett. 30, 2042. https://doi.org/10.1029/2003GL018240.

Rieckh, T., Scherllin-Pirscher, B., Ladstädter, F., Foelsche, U., 2014. Characteristics of tropopause parameters as observed with GPS radio occultation. Atmos. Meas. Tech. 7, 3947–3958. https://doi.org/10.5194/amt-7-3947-2014.

Schweiger, A.J., Lindsay, R.W., Vavrus, S., Francis, J.A., 2008. Relationships between Arctic Sea ice and clouds during autumn. J. Clim. 21 (18), 4799–4810. https://doi.org/10.1175/2008JCLI2156.1.

Shupe, M.D., Walden, V.P., Eloranta, E., Uttal, T., Campbell, J.R., Starkweather, S.M., Shiobara, M., 2011. Clouds at Arctic atmospheric observatories. Part I: occurrence and macrophysical properties. J. Appl. Meteorol. Climatol. 50 (3), 626–644. https://doi.org/10.1175/2010JAMC2467.1.

Son, S.-W., Tandon, N.F., Polvani, L.M., 2011. The fine-scale structure of the global tropopause derived from COSMIC GPS radio occultation measurements. J. Geophys. Res. Atmos. 116, D20113. https://doi.org/10.1029/2011JD016030.

Sotiropoulou, G., Sullivan, S., Savre, J., Lloyd, G., Lachlan-Cope, T., Ekman, A.M.L., Nenes, A., 2020. The impact of secondary ice production on Arctic stratocumulus. Atmos. Chem. Phys. 20, 1301–1316. https://doi.org/10.5194/acp-20-1301-2020.

Vitart, F., Anderson, J.L., Stern, W.F., 1997. Simulation of interannual variability of tropical storm frequency in an ensemble of GCM integrations. J. Clim. 10, 745–760. https://doi.org/10.1175/1520-0442(1997)010%3C0745:SOIVOT%3E2.0.CO;2.

Voigt, C., Schlager, H., Ziereis, H., Kärcher, B., Luo, B.P., Schiller, C., Krämer, M., Popp, P.J., Irie, H., Kondo, Y., 2006. Nitric acid in cirrus clouds. Geophys. Res. Lett. 33, L05803. https://doi.org/10.1029/2005GL025159.

Wargan, K., Coy, L., 2016. Strengthening of the tropopause inversion layer during the 2009 sudden stratospheric warming: a MERRA-2 study. J. Atmos. Sci. 73 (5), 1871–1887. Retrieved Jun 16, 2022, from. https://journals.ametsoc.org/view/journals/atsc/73/5/jas-d-15-0333.1.xml.

Weisz, E., Li, J., Menzel, W.P., Heidinger, A.K., Kahn, B.H., Liu, C.-Y., 2007. Comparison of AIRS, MODIS, CloudSat and CALIPSO cloud top height retrievals. Geophys. Res. Lett. 34, L17811. https://doi.org/10.1029/2007GL030676.

Winker, D., Hunt, W., Weimer, C., 2017. The on-orbit performance of the CALIOP LIDAR on CALIPSO. In: International Conference on Space Optics—ICSO 2008, Vol. 10566. International Society for Optics and Photonics, p. 105661H. https://doi.org/10.1117/12.2308248.

WMO, 1957. Meteorology-A Three-Dimensional Science, Vol. 6. WMO Bull, Geneva, Switzerland, pp. 134–138.

Xian, T., Homeyer, C.R., 2019. Global tropopause altitudes in radiosondes and reanalyses. Atmos. Chem. Phys. 19, 5661–5678. https://doi.org/10.5194/acp-19-5661-2019.

Yang, Q., Fu, Q., Hu, Y., 2010. Radiative impacts of clouds in the tropical tropopause layer. J. Geophys. Res. Atmos. 115, D00H12. https://doi.org/10.1029/2009JD012393.

Yeo, H., Park, S.-J., Kim, B.-M., Shiobara, M., Kim, S.-W., Kwon, H., Kim, J.-H., Jeong, J.-H., Park, S.S., Choi, T., 2018. The observed relationship of cloud to surface longwave radiation and air temperature at Ny-Ålesund, Svalbard. Tellus Ser. B Chem. Phys. Meteorol. 70, 1–10. https://doi.org/10.1080/16000889.2018.1450589.

Yeo, H., Kim, M.-H., Son, S.-W., Jeong, J.-H., Yoon, J.-H., Kim, B.-M., Kim, S.-W., 2022. Arctic cloud properties and associated radiative effects in the three newer reanalysis datasets (ERA5, MERRA-2, JRA-55): discrepancies and possible causes. Atmos. Res. 270, 106080 https://doi.org/10.1016/j.atmosres.2022.106080.

Young, S.A., Vaughan, M.A., Garnier, A., Tackett, J.L., Lambeth, J.D., Powell, K.A., 2018. Extinction and optical depth retrievals for CALIPSO's Version 4 data release. Atmos. Meas. Tech. 11, 5701–5727. https://doi.org/10.5194/amt-11-5701-2018.